

# PHASE-SENSITIVE HOLOGRAPHY OF SOLAR ACTIVITY

D. C. BRAUN<sup>\*,†</sup> and C. LINDSEY

*Solar Physics Research Corporation, 4720 Calle Desecada, Tucson, AZ 85718, U.S.A.*

*e-mails: dbraun@solar.stanford.edu; lindsey@sprc.com*

(Received 27 September 1999; accepted 28 January 2000)

**Abstract.** Phase-correlation statistics comparing acoustic radiation coming out of a particular point on the solar photosphere with acoustic radiation going into it show considerably reduced sound travel times through the subphotospheres of active regions. We have now applied techniques in phase-sensitive seismic holography to data from the Solar Oscillations Investigation – Michelson Doppler Imager (SOI-MDI) on the Solar and Heliospheric Observatory (SOHO) spacecraft to obtain high resolution phase-correlation maps of a large, complex active region and the ‘acoustic moat’ which surrounds it. We report the following new results: First, the reduced sound travel-time perturbations in sunspots, acoustic moats, and isolated plages increase approximately in proportion to the logarithm of the surface magnetic flux density, for flux densities above 10 G. This is consistent with an interpretation of the travel-time anomalies, observed with holographic and other local-helioseismic procedures, as caused by acoustic Wilson-like depressions in photospheres of magnetic regions. Second, we find that, compared with isolated plages, the acoustic moats have an additional sound travel-time reduction on the order of 3–5 s which may be explained by a thermal excess due to the blockage of convective transport by the sunspot photosphere. Third, the combined effect of the Wilson depression in plages, acoustic moats, and sunspots may explain the observed variation of global  $p$ -mode frequencies with the solar cycle. Fourth, we find that active regions, including sunspots, acoustic moats, and plages, significantly reflect  $p$  modes above the acoustic cut-off frequency, where the surface of the quiet Sun acts as a nearly perfect absorber of incident acoustic radiation.

## 1. Introduction

The discovery, made over a decade ago, that sunspots and solar active regions are strong absorbers of incident acoustic ( $p$ -mode) radiation (Braun, Duvall, and LaBonte, 1987, 1988) provided the primary impetus for the development of phase coherent helioseismic imaging concepts (Lindsay and Braun, 1990, 1997; Braun *et al.*, 1992; Lindsey *et al.*, 1996) which were specifically designed to probe the three-dimensional distribution of local acoustic perturbations within the solar interior. In the past two years, the application of seismic holography to observations from the Solar Oscillation Investigation – Michelson Doppler Imager (SOI-MDI) aboard the Solar and Heliospheric Observatory (SOHO) spacecraft has proceeded

<sup>\*</sup>Visitor, Joint Institute for Laboratory Astrophysics, University of Colorado, Boulder, CO 80309-0440, U.S.A.

<sup>†</sup>Current mailing address: Colorado Research Associates, 3380 Mitchell Lane, Boulder, CO 80301, U.S.A.



to uncover a remarkable array of new solar acoustic phenomena. These have included the discoveries of the ‘acoustic moat’ (Lindsey and Braun, 1998a; Braun *et al.*, 1998), ‘acoustic condensations’ (Lindsey and Braun, 1998b; Braun and Lindsey, 1999), the ‘acoustic glory’ (Braun and Lindsey, 1999) and the first helioseismic images of a solar flare (Donea, Braun, and Lindsey, 1999). A review of the scientific accomplishments of helioseismic holography is given elsewhere in this volume (Braun and Lindsey, 2000).

The first major discovery from seismic holography was that of the acoustic moat, a region showing a general deficit of 10–30% in 3–4 mHz acoustic radiation which extends *far beyond* sunspots, over distances 30–60 Mm beyond their penumbrae (Braun *et al.*, 1998). Although the acoustic moat may have its own absorption mechanism, it is possible that it simply scatters, by means of Doppler or thermal perturbations within it, the acoustic deficit introduced by the sunspot. Braun *et al.* (1998) and Lindsey and Braun (1998a) proposed that the acoustic moat signifies an anomalous convection cell flowing rapidly outwards not far beneath the solar surface, driven by heat accumulation caused by the blockage of convective transport through the sunspot photosphere. In this work we apply ‘phase-sensitive holography’ to SOI-MDI observations of a complex active region to look for thermal signatures of the acoustic moat. We begin with a brief description of helioseismic holography and the development of phase-sensitive diagnostics of sound travel-time perturbations in the near solar interior.

## 2. Phase-Sensitive Holography

Helioseismic holography is the phase-coherent wave-mechanical regression of the  $p$ -mode acoustic field into the solar interior based on helioseismic observations at the solar surface (Lindsey and Braun, 1997). Given a database that expresses the surface acoustic signal in terms of a field amplitude,  $\psi(\mathbf{r}', t')$ , the task can be expressed in terms of the computation of the acoustic ‘egression’ and ‘ingression’,  $H_+(z, \mathbf{r}, t)$  and  $H_-(z, \mathbf{r}, t)$ , at depth  $z$  beneath horizontal location  $\mathbf{r}$ , at time  $t$ :

$$H_+(z, \mathbf{r}, t) = \int dt' \int_{a < |\mathbf{r} - \mathbf{r}'| < b} d^2\mathbf{r}' \psi(\mathbf{r}', t') G_+(z, \mathbf{r}, t, \mathbf{r}', t'), \quad (1)$$

$$H_-(z, \mathbf{r}, t) = \int dt' \int_{a < |\mathbf{r} - \mathbf{r}'| < b} d^2\mathbf{r}' \psi(\mathbf{r}', t') G_-(z, \mathbf{r}, t, \mathbf{r}', t'). \quad (2)$$

The Green’s function  $G_+$  represents the subsurface disturbance at  $(z, \mathbf{r}, t)$  resulting from a unit acoustic impulse originating at surface coordinates  $(0, \mathbf{r}', t')$ .  $G_-$  is the time-reverse counterpart of  $G_+$ . The Green’s functions are computed at the desired focal-plane depth,  $z$ , from a standard solar model. In our application, the computation is confined to an annular ‘pupil’ surrounding the ‘focal point’,  $\mathbf{r}$ , whose inner radius  $a = 15$  Mm and outer radius  $b = 45$  Mm.

In *acoustic power holography* one integrates the square of the egression amplitude over a time-span  $\Delta T$  to yield maps of the acoustic egression power at depth  $z$ :

$$P_+(z, \mathbf{r}) = \int_{\Delta T} dt |H_+(z, \mathbf{r}, t)|^2 . \quad (3)$$

This diagnostic is sensitive to significant acoustic sources and sinks. A substantially anisotropic acoustic illumination, such as from nearby strong acoustic absorbers like sunspots, can also render nearby scatterers visible in egression power maps.

Lindsey and Braun (1997) describe phase-sensitive diagnostics of acoustical perturbations that simply refract or scatter acoustic radiation in an ambient medium that is spatially isotropic. These techniques offer an appraisal of the phase shifts due to refraction and Doppler effects caused by flows. An example of such a diagnostic is the computation of the temporal correlation between the egression and ingression amplitudes:

$$C(z, \mathbf{r}, \tau) = \int_{\Delta T} dt H_-(z, \mathbf{r}, t) H_+(z, \mathbf{r}, t + \tau) . \quad (4)$$

A localized refractive perturbation at the point  $(z, \mathbf{r})$  will manifest a time delay between the egression and ingression amplitudes, shifting the peak of the correlation function  $C$  from  $\tau = 0$ . Maps of the time delays,  $\tau$ , over the solar surface ( $z = 0$ ), for example, render perturbations characteristic of travel-time variations caused by wave-speed anomalies and Wilson-like depressions due to magnetic fields. Chen *et al.* (1998) have applied this technique to observations from the Taiwan Oscillation Network (TON). In this study we apply phase-sensitive diagnostics to SOI-MDI observations of a large active region with an extended acoustic moat.

For the purpose of improved numerical efficiency, the computations reported here were made in the ‘spectral perspective’ (Lindsey and Braun, 1997) which directly renders the temporal Fourier transforms,  $\hat{H}_+(\mathbf{r}, \nu)$  and  $\hat{H}_-(\mathbf{r}, \nu)$ , of the single-skip egression,  $H_+(\mathbf{r}, t)$ , and ingression,  $H_-(\mathbf{r}, t)$ , respectively, where  $\nu$  is the temporal frequency. We omit the argument  $z$  since the computations in this study are performed at the surface. The correlation theorem then provides that

$$\hat{C}(\mathbf{r}, \nu) = \hat{H}_-^*(\mathbf{r}, \nu) \hat{H}_+(\mathbf{r}, \nu) , \quad (5)$$

where  $\hat{C}$  is the temporal Fourier transform of the correlation  $C$  and the asterisk denotes the complex conjugate. The spectral domain facilitates the chromatic analysis of the refractive perturbations wherein we examine the phase of  $\hat{C}(\mathbf{r}, \nu)$  as a function of frequency. As in prior studies (Donea, Braun, and Lindsey, 1999; Donea, Lindsey, and Braun, 2000) the egression and ingression computations were made with Green’s functions that take full account of dispersion of the acoustic spectrum by the near subphotosphere (see Lindsey and Braun, 2000).

### 3. Data and Results

The SOI-MDI data analyzed in this study consist of nearly continuous full-disk Doppler images obtained once per minute over the 24-hr period 15–16 March 1998 while a large, growing active-region (NOAA AR 8179) was close to the central meridian. The SOI-MDI and its data products are described by Scherrer *et al.* (1995). Figure 1(a) shows a contemporary SOI-MDI continuum image. Figure 1(b) is an average of several individual SOI-MDI magnetograms made over the 24-hr period, and Figure 1(c) shows the log of  $B^2$ , where  $B$  is the observed magnetic flux density.

Figures 1(d) and 1(e) show egression power maps of the region, computed for a focal plane located at the solar surface, and processed to include only acoustic radiation within a 1 mHz bandpass centered at 5 and 3 mHz, respectively. A ‘flat fielding’ operation, which involves dividing the egression by a smeared version of the ingression map, is used to correct for artifacts introduced by local variations of the acoustic wave signature in magnetic regions (Lindsey and Braun, 1999).

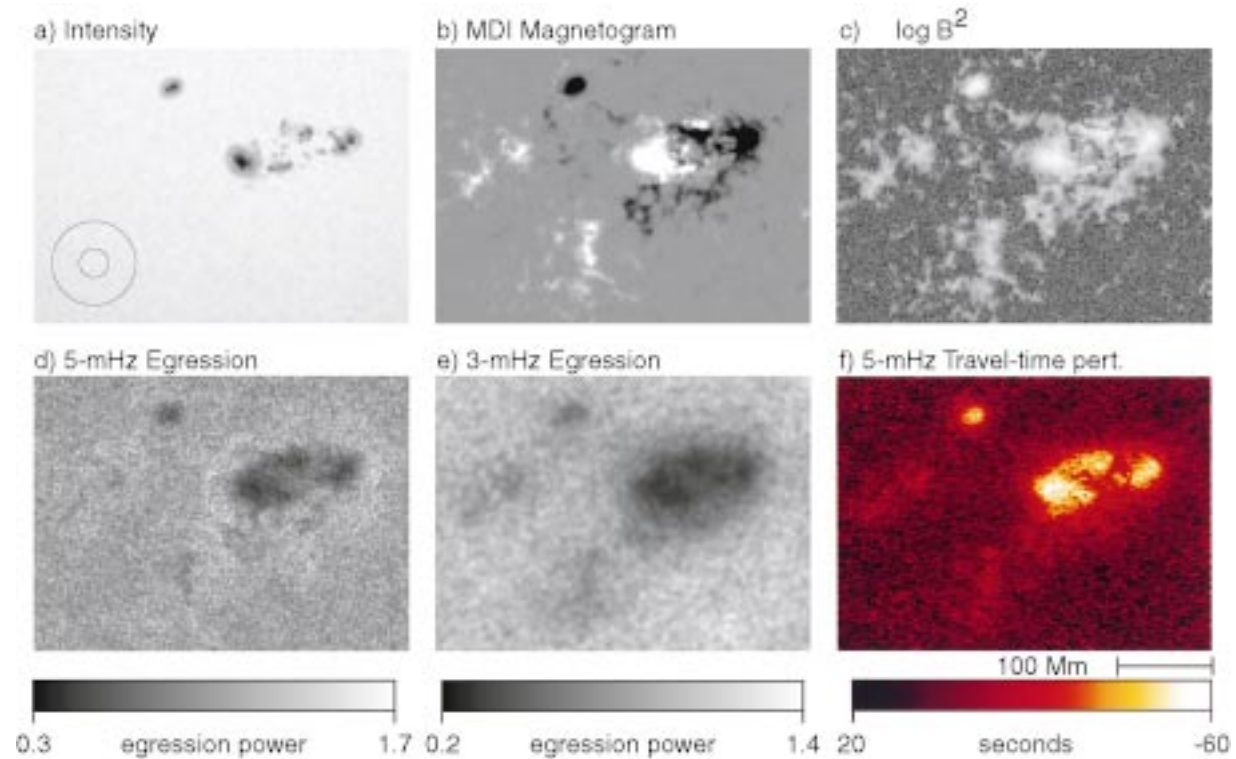
Acoustic moats are characterized by halos of egression power deficit seen in the 3 mHz map (Figure 1(e)) extending outside of magnetic regions (Braun *et al.*, 1998; Lindsey and Braun, 1998a). At higher temporal frequencies (Figure 1(d)), the acoustic deficit at the periphery of the moat is replaced by a halo of *excess* emission, called the ‘acoustic glory’, which is particularly prominent in complex active regions (Braun and Lindsey, 1999; Donea, Lindsey, and Braun, 2000).

Figure 1(f) shows a map of the sound travel-time perturbations determined from the correlation between the egression and ingression amplitudes (Equation (5)). The ‘one-way’ travel-time perturbation  $\delta t$  is given by

$$\delta t(\mathbf{r}) = \frac{1}{2} \frac{1}{2\pi\nu_0} \arg \left( \int_{\Delta\nu} \hat{C}(\mathbf{r}, \nu) d\nu \right), \quad (6)$$

where  $\Delta\nu$  is a selected frequency bandpass centered at  $\nu_0$ . For the example shown in Figure 1(f), the travel-time perturbations were computed for a 1 mHz bandpass centered at 5 mHz. *Bright* regions indicate one-way travel times *less than* the mean quiet Sun, for which  $\delta t = 0$ .

Travel-time reductions up to one minute are seen in sunspots, and significant but smaller reductions are visible in the region occupied by the acoustic moats surrounding the spots as well as in isolated plages located to the left and lower left of the main active region. Unlike the 3 mHz egression power signature, however, the sound travel-time anomalies correlate sharply with surface magnetic regions. There is a distinctive similarity in appearance between the the map of travel-time anomalies (Figure 1(f)) with that of the log of the surface magnetic flux density (Figure 1(c)). Figure 2 shows scatter-plots of travel-time perturbations for selected regions against the log of  $|B|$ . The top two panels of Figure 2 (‘sunspots’) represent points located within a region encompassing the visible sunspots in the main active



*Figure 1.* (a) shows an MDI continuum intensity image of AR 8179 taken 1998 March 15.0. (b) is an average of three magnetograms over the subsequent 24-hr period, and (c) illustrates the logarithm of the square of the magnetogram. The areas enclosed by the curves in (b) indicate regions discussed in the text. The greyscale used in (b) saturates below  $-300$  G and above  $+300$  G. The greyscale used in (c) spans a range of magnetic flux density between 0.3 and 1600 G. (d) and (e) show egression power maps of the region, at 5 and 3 mHz, respectively. The greyscales indicate egression power, normalized to unity for the quiet Sun. (f) shows a map of 5 mHz sound travel-time perturbations, with respect to the quiet Sun. The annulus in (a) shows the dimensions of the pupil of both ingress and egression computations.

region, as enclosed by the solid curve in Figure 1(b), and for which  $|B| > 100$  G. The lower two panels ('moat') represent points located between the inner (solid) curve and the outer (dotted) curve shown in Figure 1(b). Travel-time perturbations observed for 3 and 5 mHz acoustic radiation are shown in the left and right panels of Figure 1, respectively. For both the sunspots and the acoustic moats, it is observed that there is a correlation of the observed sound travel-time perturbations with  $|B|$ , with an approximately linear dependence of the travel time with the log of the observed magnetic flux density.

These results suggest that much of the reduced sound travel times in active regions measured with other local helioseismic techniques, including Hankel analysis (Braun, 1995; Fan, Braun, and Chou, 1995) time-distance correlations (Duvall *et al.*, 1996; Kosovichev, 1996; Braun, 1997), and ring-diagram analysis (Hindman *et al.*, 2000), may be attributable to an 'acoustic Wilson depression' that applies to all surface magnetic regions. The presence of magnetic fields in the photosphere of active regions reduces the gas pressure relative to its value in magnetically free regions, effectively displacing the density variation with height of the magnetic region downward with respect to the quiet Sun. Magnetic fields thereby indicate effective dips in the solar surface. In an atmosphere in which the pressure increases exponentially with depth, the displacement will be proportional to the log of the applied magnetic pressure. For sunspots, the Wilson depression is observed to be as deep as 300 km, which corresponds to a one-way  $p$ -mode travel-time reduction of approximately 40 s. This value is comparable to the largest perturbations observed in the umbrae of sunspots, as indicated by Figures 2(a) and 2(b).

While the effect of the Wilson depression may apparently be a major source of the travel-time reductions observed in active regions, it seems that a significant fraction of the reduction observed in the acoustic moats may be attributable to a sound-speed enhancement below the surface. Evidence for this is shown in Figure 3, which compares the mean travel-time perturbation in the acoustic moat, previously shown in Figures 2(c) and 2(d), with the travel times observed in an isolated plage, enclosed by the dashed curve shown in Figure 1(b). For clarity, the individual pixel values are not plotted, but are instead averaged over bins of magnetic flux density and represented by vertical bars indicating the standard error of the mean. It is apparent that the acoustic moats exhibit an additional sound travel-time reduction, on the order of 4 and 5 s at 3 and 5 mHz, respectively, compared with the plages. This additional travel-time anomaly is *quite independent* of the value of the surface magnetic flux density. We suggest that this component of the travel-time perturbation in acoustic moats may be explained by enhanced sound speeds due to a thermal excess below the moat. This would be a natural result of blockage of convective transport in the underlying sunspot photosphere.

It is worth emphasizing that both the plage and the moat exhibit a significant travel-time reduction for 3-mHz acoustic radiation, particularly at higher magnetic flux densities. This has important implications for understanding the solar-cycle variations of global-mode frequencies. Cunha, Brüggen, and Gough (1998) suggest

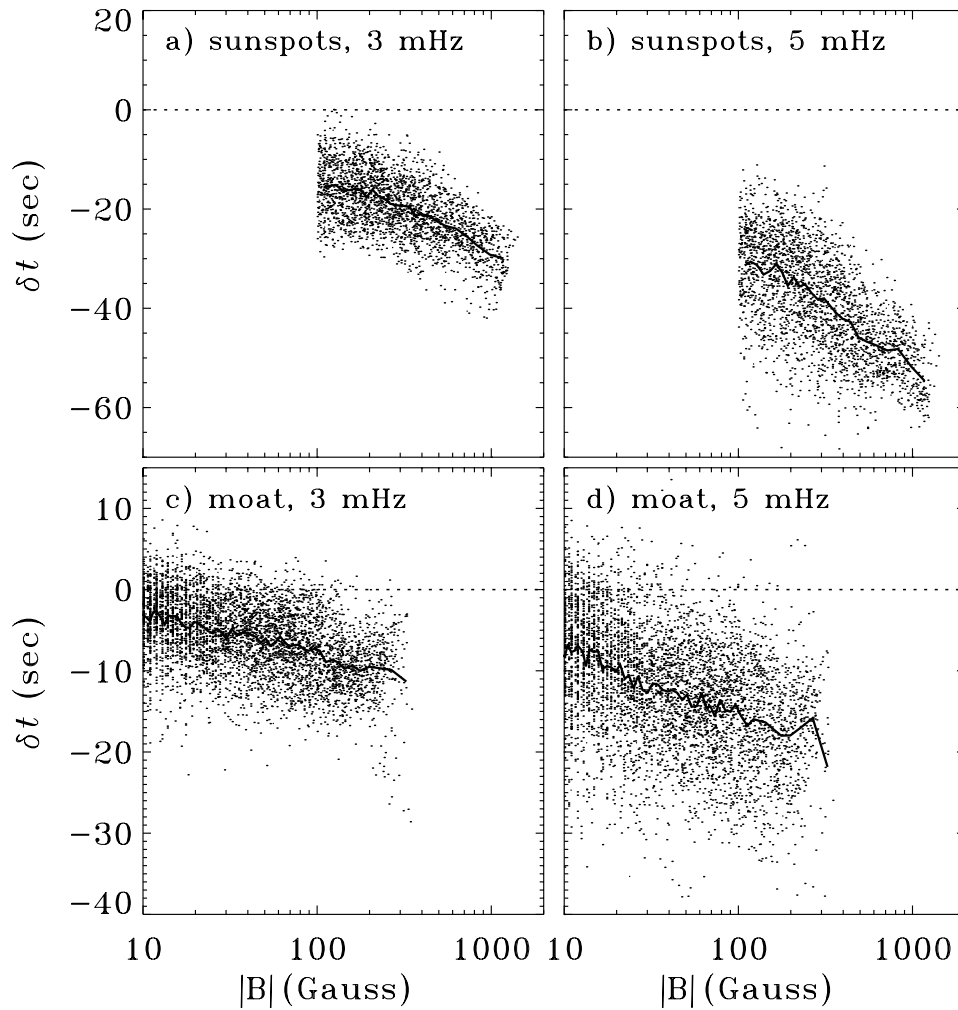


Figure 2. The points indicate individual measurements of the sound travel-time perturbations ( $\delta t$ ) for 3 mHz (left panels) and 5 mHz (right panels) plotted against the surface magnetic flux density. The upper two panels ('sunspots') show the results for points contained within the solid curve superimposed on the magnetogram in Figure 1(b), and for which  $|B| > 100$  G. The bottom panels ('moat') show the points lying between the solid and dotted curves in Figure 1(b). The solid lines indicate the mean of  $\delta t$  binned over small intervals of magnetic flux density.

that sound travel-time perturbations within sunspots alone could provide a significant contribution to the global-mode frequency differences observed between solar minima and solar maxima. Following their work (cf., Equation (9) of Cunha, Brüggen, and Gough, 1998), we estimate the frequency shift  $\delta\nu_{\ell mn}$  of a  $p$  mode, with degree  $\ell$ , azimuthal order  $m$ , and radial order  $n$ , associated with a local surface travel time perturbation  $\delta t$  distributed over the solid angle  $\Omega$ , by

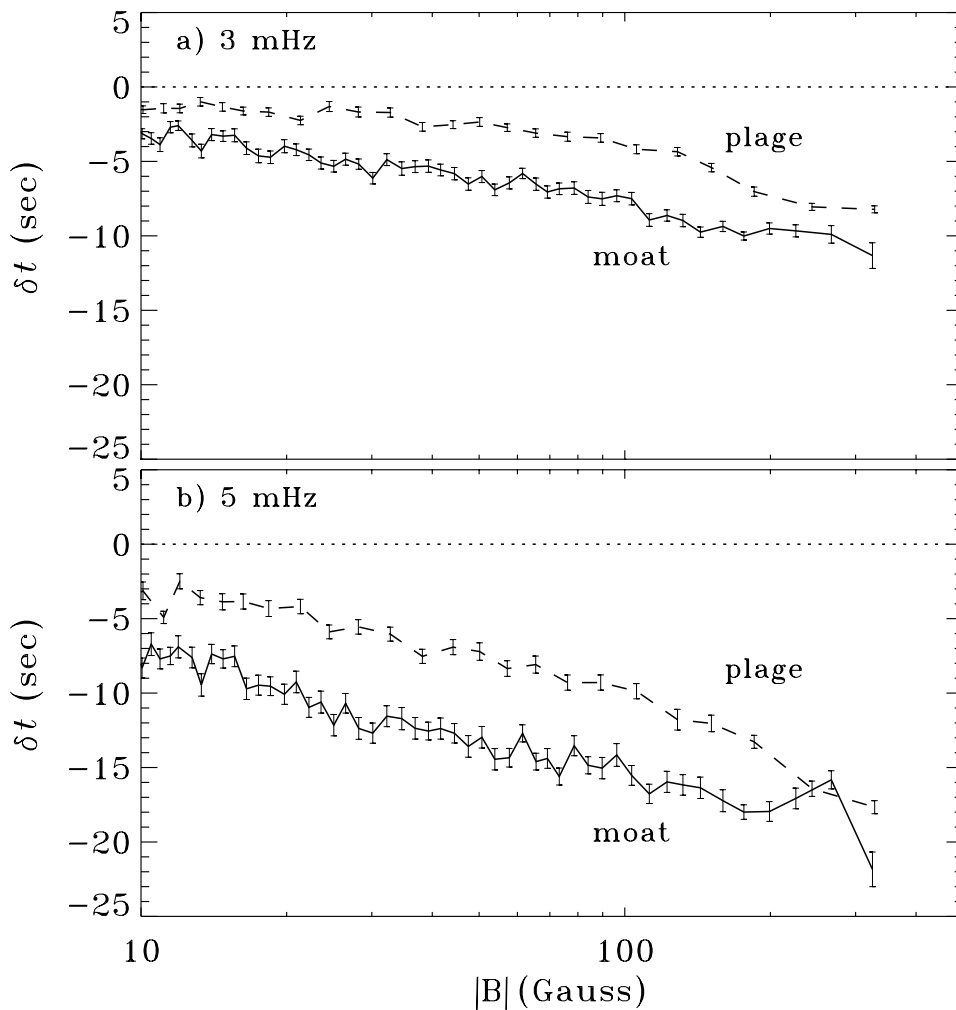


Figure 3. Mean travel-time perturbations at 3 mHz (a) and 5 mHz (b) plotted against the surface magnetic flux density. The dashed lines connect the values observed within the isolated plages contained within the dashed curve shown in Figure 1(b) and the solid lines represent the mean perturbations for the moat as previously shown in Figure 2.

$$\frac{\delta v_{\ell mn}}{v_{\ell mn}} \approx -\frac{2}{\tau_{\ell n}} \int_{4\pi} [Y_{\ell}^m]^2 \delta t \, d\Omega, \quad (7)$$

where  $\tau_{\ell n}$  is the time for a  $p$  mode to propagate from the upper turning point of its acoustic cavity to the lower turning point and back, and  $Y_{\ell}^m$  is a spherical harmonic. Using Equation (7) we find that the observed travel time perturbations at 3 mHz, integrated over the field of view shown in Figure 1, yields a value of  $\delta v/v \approx 1.2 \times 10^{-5}$  for radial ( $\ell = 0$ )  $p$  modes. This global-mode frequency perturbation, due to a *single active region complex*, is about 0.1 of the total observed variation in the observed frequencies from solar minimum to maximum

(e.g., Jiménez-Reyes *et al.*, 1998). In the immediate vicinity of AR 8179, we find that the relative contributions from sunspots, acoustic moats and the plages to the integral in the numerator in Equation (7) are approximately 50%, 30%, and 20%, respectively. Over the entire solar surface, we expect that the contribution from the plages dominates the integrated travel-time perturbation, since they have a filling factor which typically exceeds that of sunspots by a factor of  $\sim 20$  (e.g., Foukal, 1998). It is therefore plausible that the combined contribution of Wilson-like depressions in plages and sunspots, and the travel-time perturbations in acoustic moats, can account for most, if not all, of observed  $p$ -mode frequency variation with the solar cycle. This result is also relevant to the local frequency shifts of high-degree  $p$  modes in active regions recently detected with ring-diagram analysis (Hindman *et al.*, 2000) and to the global-mode frequency-shift analysis of Howe, Komm, and Hill (1999).

Application of phase-sensitive holography at high temporal frequencies reveals that active regions reflect a significant fraction of incident acoustic radiation above the acoustic cut-off frequency of the quiet Sun photosphere. This is illustrated in travel-time maps made using  $p$  modes at different temporal frequencies between 3 and 6 mHz (Figure 4). The travel-time anomaly observed in the active regions is clearly visible at all temporal frequencies, including frequencies well above the acoustic cut-off frequency ( $\sim 5.3$  mHz) where the surface of the quiet Sun becomes a nearly perfect absorber of incident acoustic radiation. At 6 mHz, the correlation between the acoustic ingression and egression amplitudes essentially vanishes in the quiet Sun, and the remaining noise yields large, random fluctuations in phase which appear in Figure 4(d). However, sunspots, plages, and acoustic moats show a well defined signature at 6 mHz indicating a strong correlation. This is the result of a significant reflection of the incident acoustic radiation by the active regions into the egression pupil.

#### 4. Discussion

A comparison between phase-correlation maps of acoustic moats with those of isolated plages has shown that the moats are characterized by a reduction in sound travel-time exceeding that exhibited by the Wilson-depression effect in plages of similar flux density. These results are consistent with a sound-speed enhancement below the photosphere of the acoustic moat.

The hydrodynamics that give rise to the acoustic moat must be complex. The gases that comprise the sunspot photosphere are far cooler than those of the surrounding quiet Sun, and without constraints maintained by magnetic forces would sink directly into the solar interior. Parker (1979) suggests that some fraction of these gases do indeed slip between magnetic flux-tube elements and engender local downdrafts. However, the proposition that the cool sunspot photosphere is a result of inhibited convection would seem to prevent such a downdraft from

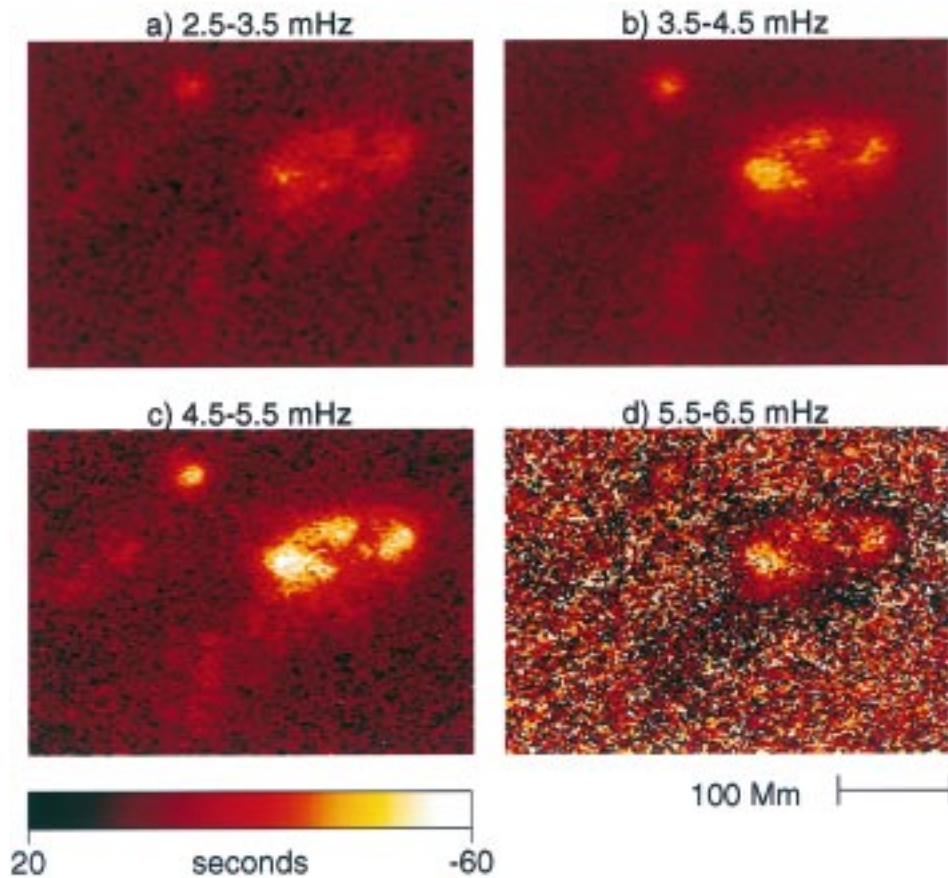


Figure 4. Maps of the sound travel-time perturbations computed over 1 mHz bandpasses centered at frequencies of 3, 4, 5, and 6 mHz.

predominating the hydromechanical flow pattern beneath the sunspot. The major direct consequence of suppressed convection in the sunspot photosphere and below must be an *accumulation of excess heat* directly beneath the sunspot photosphere. Such an accumulation will certainly alter the thermal structure of the environment surrounding the sunspot, with a strong tendency to cause a strong, hot *updraft and outflow* from the periphery of the sunspot (Figure 5). Wilson (1979), Meyer *et al.* (1974), Nye, Bruning, and LaBonte (1988), and Fox, Sofia, and Chan (1991) suggest the need for anomalous convection in the near sunspot interior to explain the thermal structure of the sunspot environment. The thermal perturbation caused by the local blockage of convective transport directly beneath the sunspot would drive a convective eddy surrounding the sunspot. Without such an eddy, the heat flux blocked by the sunspot should appear in a compact bright ring surrounding the sunspot, as a result of standard convective diffusion (Parker, 1974). This ring would have an intensity considerably greater than that characterizing the weak emission

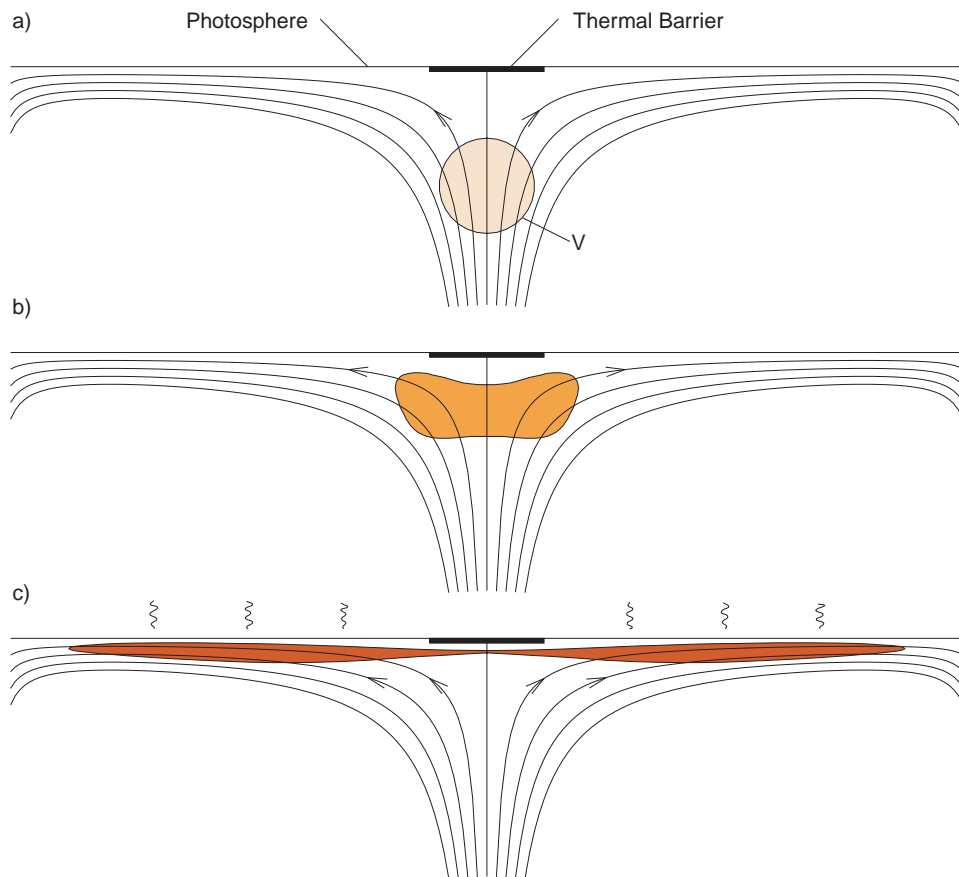


Figure 5. A schematic representation of a convective eddy driven by the local blockage of convective transport by a thermal barrier at the surface (solid rectangle). (a)–(c) show the temporal evolution of a thermal excess indicated initially by the volume  $V$  in (a).

that is actually observed (Rast *et al.*, 1999). Lindsey and Braun (1998a) proposed that the basic subsurface morphology of such an eddy could spread the thermal excess initially accumulated in a volume  $V$  (Figure 5(a)) into a relatively thin region surrounding the blockage (Figure 5(c)). The relative buoyancy of the thermal excess would assure continued spreading until it is allowed to access the solar surface efficiently through normal supergranular convection. This would explain the remarkable horizontal extent of the acoustic moat.

Sheeley (1969, 1972), Harvey and Harvey (1973), and Brickhouse and LaBonte (1988) have established that sunspots can have strong surface and probably near subsurface outflows. Lindsey *et al.* (1996) suggest that these flows extend substantially beneath the surface.

It should be realized that these results are in apparent conflict with downflows inferred from the time-distance measurements of Duvall *et al.* (1996), which suffer

from uncertainties introduced by the use of observations within sunspots (see, for example, Braun, 1997). Lindsey and Braun (1997) describe extensions of phase-sensitive holography that are diagnostic of horizontal flows. These holographic measurements, like those reported in this study, can be fashioned to rely on waves measured outside of the region that is being diagnosed. This avoids phase errors introduced by the active region photosphere.

### Acknowledgements

We greatly appreciate the support we have gotten from the SOHO SOI-MDI team and the fine quality of the data which they have given us. We especially appreciate the conscientious support of Dr P. Scherrer, head of the SOHO-MDI project. SOHO is a project of international cooperation between ESA and NASA. D.C.B., a visitor at the Joint Institute for Laboratory Astrophysics, is grateful to Ellen Zweibel and the staff of JILA for their hospitality and support. This research is supported by NSF Grant AST 9528249 and NASA Grant NAG5-7236 through SPRC, and by the SOI-MDI NASA investigation through JILA.

### References

- Braun, D. C.: 1995, *Astrophys. J.* **451**, 859.  
 Braun, D. C.: 1997, *Astrophys. J.* **487**, 447.  
 Braun, D. C. and Lindsey, C.: 1999, *Astrophys. J.* **513**, L79.  
 Braun, D. C. and Lindsey, C.: 2000, *Solar Phys.* **192**, 285 (this issue).  
 Braun, D. C., Duvall, T. L. Jr., and LaBonte, B. L.: 1987, *Astrophys. J.* **319**, L27.  
 Braun, D. C., Duvall, T. L. Jr., and LaBonte, B. L.: 1988, *Astrophys. J.* **335**, 1015.  
 Braun, D. C., Lindsey, C., Fan, Y., and Jefferies, S. M.: 1992, *Astrophys. J.* **392**, 739.  
 Braun, D. C., Lindsey, C., Fan, Y., and Fagan, M.: 1998, *Astrophys. J.* **502**, 968.  
 Brickhouse, N. S. and LaBonte, B. J.: 1988, *Solar Phys.* **115**, 43.  
 Chen, H.-R., Chou, D.-Y., Chang, H.-S., Sun, M. T., Yeh, S.-J., LaBonte, B., and the TON Team: 1998, *Astrophys. J.* **501**, L139.  
 Cunha, M., Brüggem, M., and Gough, D. O.: 1998, in S. G. Korzennik and A. Wilson (eds.), *Structure and Dynamics of the Interior of the Sun and Sun-like Stars*, ESA, SP-418, p. 905.  
 Donea, A.-C., Braun, D. C., and Lindsey, C.: 1999, *Astrophys. J.* **513**, L143.  
 Donea, A.-C., Lindsey, C., and Braun, D. C.: 2000, *Solar Phys.* **192**, 321 (this issue).  
 Duvall, T. L. Jr., D'Silva, S., Jefferies, S. M., Harvey, J. W., and Schou, J.: 1996, *Nature* **379**, 235.  
 Fan, Y., Braun, D. C., and Chou D.-Y.: 1995, *Astrophys. J.* **451**, 877.  
 Foukal, P.: 1998, *Astrophys. J.* **500**, 958.  
 Fox, P. A., Sofia, S. C., and Chan K. L.: 1991, *Solar Phys.* **135**, 15.  
 Harvey, K. and Harvey, J.: 1973, *Solar Phys.* **28**, 61.  
 Hindman, B. W., Haber, D. A., Toomre, J., and Bogart, R.: 2000, *Solar Phys.* **192**, 363 (this issue).  
 Howe, R., Komm, R., and Hill, F.: 1999, *Astrophys. J.* **524**, 1084.  
 Jiménez-Reyes, S. J., Régulo, C., Pallé, P. L., and Roca Cortés, T.: 1998, *Astron. Astrophys.* **329**, 1119.  
 Kosovichev, A. G.: 1996, *Astrophys. J.* **461**, L55.

- Lindsey, C. and Braun, D. C.: 1990, *Solar Phys.* **126**, 101.
- Lindsey, C. and Braun, D. C.: 1997, *Astrophys. J.* **485**, 895.
- Lindsey, C. and Braun, D. C.: 1998a, *Astrophys. J.* **499**, L99.
- Lindsey, C. and Braun, D. C.: 1998b, *Astrophys. J.* **509**, L129.
- Lindsey, C. and Braun, D. C.: 1999, *Astrophys. J.* **510**, 494.
- Lindsey, C. and Braun, D. C.: 2000, *Solar Phys.* **192**, 261 (this issue).
- Lindsey, C., Braun, D. C., Jefferies, S. M., Woodard, M. F., Fan, Y., Gu, Y., and Redfield, S.: 1996, *Astrophys. J.* **470**, 636.
- Meyer, F., Schmidt, H. U., Weiss, N. O., and Wilson, P. R.: 1974, *Monthly Notices Royal Astron. Soc.* **169**, 35.
- Nye, A., Bruning, D., and LaBonte, B. J.: 1988, *Solar Phys.* **115**, 251.
- Parker, E. N.: 1974, *Solar Phys.* **36**, 249.
- Parker, E. N.: 1979, *Astrophys. J.* **230**, 905.
- Rast, M., T., Fox, P. A., Lin, H., Lites, B. W., Meisner, R. W., and White, O. R.: 1999, *Nature* **401**, 678.
- Scherrer, P. H. *et al.*: 1995, *Solar Phys.* **162**, 129.
- Sheeley, N. R.: 1969, *Solar Phys.* **9**, 347.
- Sheeley, N. R.: 1972, *Solar Phys.* **25**, 98.
- Wilson, P. R.: 1973, *Solar Phys.* **32**, 435.